Available online at www.sciencedirect.com
SCIENCE DIRECT®
PERGAMON
International Journal of Heat and Mass Transfer 46 (2003) 1759–1771
International Journal of HEAT and MASS TRANSFER
www.elsevier.com/locate/ijhmt

Effect of surface tension on convection in a binary fluid layer under a zero gravity environment

A. Bahloul *, R. Delahaye, P. Vasseur, L. Robillard

Ecole Polytechnique, Centre Ville, C.P. 6079, Succ., Montréal, Qué., Canada H3C3A7

Received 7 June 2002; received in revised form 16 November 2002

Abstract

The Marangoni flows in a horizontal layer of a binary mixture with an undeformable free upper surface are studied analytically and numerically. The system is heated and cooled by constant heat fluxes. The surface tension is assumed to vary linearly with temperature and solute concentration. Both double diffusive convection and Soret induced convection, in a zero gravity level, are considered. The governing parameters of the problem are the thermal Marangoni number Ma_T, the solutal Marangoni number Ma_S, the Prandtl and the Lewis numbers Pr and Le, the aspect ratio A and the parameter a defining the mechanism responsible for the occurrence of the solutal gradients (double diffusion or Soret effect). An approximate analytical solution, based on the parallel flow approximation, is proposed. Bifurcation diagrams are presented for the cases in which the solutal Marangoni effect acts in the same direction or competes with the thermal Marangoni effect. The stability of the parallel flow solution is studied numerically and the threshold for Hopf bifurcation determined. The validity of the analytical model is tested against the results obtained by solving numerically the full governing equations.

1. Introduction

Surface tension-driven convection in a layer of fluid heated from below or above has been considerably studied in the past since these flows are important in several material processing technologies. Applications include for example small-scale hydrodynamics [1] and motion in crystal growth melts in microgravity conditions [2]. An understanding of the physical phenomenon associated with surface tension induced convection is required in order to improve the quality of materials.

Thermocapillary flows in a pure fluid have been investigated, both theoretically and numerically, by several authors. In his pioneering work, Pearson [3] reported the critical Marangoni number for the thermocapillary instability in a fluid layer heated from below. The combined effect of surface tension and buoyancy was investigated by Nield [4] on the basis of the linear stability theory. The role of interfacial deformation of the free surface has been considered by Davis and Homsy [5], Scriven and Sternling [6] and Takashima [7], among others. Three dimensional effects have been investigated by Dauby and Lebon [8] and Bergeon et al. [9]. A recent review on the subject of thermocapillary instability is consolidated by Tomita and Abe [10].

The study of Marangoni flows has also been performed in the case of a binary mixture for which surface tension depends on both temperature and solute concentration. For this situation, the linear stability analysis of Pearson [3] was generalized by Mc Taggart [11]. The linear and nonlinear doubly-diffusive Marangoni instability in a thin liquid film was considered by Ho and Chang [12]. Nonlinear finite-amplitude instability and mode competition between oscillatory and static rolls have been discussed by these authors. The linear stability characteristics of a fluid layer with simultaneous temperature and concentration gradients in a reduced-gravity field was investigated by Chen and Su [13]. Results show that the predicted stability boundary based

* Corresponding author. Tel.: +1-514-340-4711; fax: +1-514-340-5917.
E-mail address: abahloul@polymtl.ca (A. Bahloul).
URL: http://www.meca.polymtl.ca/convection.

0017-9310/03/$ - see front matter © 2003 Elsevier Science Ltd. All rights reserved.
doi:10.1016/S0017-9310(02)00480-5

Nomenclature

A	aspect ratio of the cavity, L'/H'
a	real number
b	constant, Eq. (21)
C	dimensionless concentration, $(N - N_0)/\Delta N$
C_N	dimensionless concentration gradient in x-direction
C_T	dimensionless temperature gradient in x-direction
D	mass diffusivity of species, $m^2\,s^{-1}$
D'	thermal diffusion coefficient, $m^2\,s^{-1}\,K^{-1}$
g	gravitational acceleration, $m\,s^{-2}$
H'	height of enclosure, m
j'	solute flux per unit area, $kg\,m^{-2}\,s^{-1}$
k	thermal conductivity, $W\,m^{-1}\,K^{-1}$
L'	width of the enclosure, m
Le	Lewis number, α/D
Ma_S	solutal Marangoni number, Eq. (15)
Ma_T	thermal Marangoni number, Eq. (15)
N	dimensionless concentration of the denser component, S'/ρ_0
N_0	initial mass fraction
ΔN	characteristic dimensionless concentration
Pr	Prandtl number, v/α
q'	constant heat flux per unit area, $W\,m^{-2}$
S'	concentration of the denser component, $kg\,m^{-3}$
t	dimensionless time, $t'\alpha/H'^2$
T	dimensionless temperature, $(T' - T'_0)/\Delta T'$
$\Delta T'$	characteristic temperature, $q'H'/k$
u	dimensionless velocity in x-direction, $u'H'/\alpha$
v	dimensionless velocity in y-direction, $v'H'/\alpha$
x	dimensionless coordinate axis, x'/H'
y	dimensionless coordinate axis, y'/H'

Greek symbols

α	thermal diffusivity, $m^2\,s^{-1}$
γ_N	solutal surface tension gradient
γ_T	thermal surface tension gradient, K^{-1}
μ	dynamic viscosity of fluid, $kg\,m^{-1}\,s^{-1}$
v	kinematic viscosity of fluid, $m^2\,s^{-1}$
θ	dimensionless temperature field, Eq. (17)
ρ	density of fluid, $kg\,m^{-3}$
$(\rho C)_f$	heat capacity of fluid, $W\,s\,m^{-3}\,K^{-1}$
σ	fluid surface tension coefficient
Ψ	dimensionless stream function, Ψ'/α

on Marangoni effects alone is completely altered in the presence of buoyancy effects induced by low gravity levels. Marangoni convection in binary mixtures with Soret effect has been considered by Joo [14]. The gravitational effects were neglected and the interface was allowed to deform. It was demonstrated that oscillatory instability can exist when the thermocapillarity is destabilizing and the solutocapillarity is stabilizing. Marangoni convection in binary mixtures with Soret effect was considered by Bergeron et al. [15,16] for a fluid layer with one undeformable free surface. Computed bifurcation diagrams show a marked transition from a weakly convective Soret regime to a strongly convective Marangoni regime when the threshold for pure fluid thermal convection is passed. Doubly diffusive Marangoni convection has also been investigated by Jue [17] and Arafune and Hirata [18]. Numerical results for the flow fields as well as temperature and concentration distributions were carried out. The Marangoni effect was found to affect considerably the flow pattern depending on whether the surface tension induced circulation and buoyancy induced circulation are in the same direction or not.

In the present paper, we consider Marangoni convection in a binary fluid layer with the horizontal boundaries heated and cooled by constant heat fluxes. The paper is organized as follows. In the next sections, the formulation of the problem and numerical method are presented. An approximate analytical solution is then proposed. This is followed by a presentation of bifurcation diagrams for both double diffusive and Soret induced convection. A linear stability analysis of the finite amplitude convection, predicted by the analytical model, is then conducted. The last section contains some concluding remarks.

2. Mathematical formulation

The physical model considered here is a horizontal cavity of width L' and height H' such that the aspect ratio A is defined as: $A = L'/H'$ (see Fig. 1). Neumann boundary conditions are applied for temperature on the horizontal walls while the vertical sides of the boundaries are assumed adiabatic. All the boundaries of the cavity, except the upper free surface, are supposed to be rigid and impermeable. The cavity is filled with a binary mixture having a uniform initial mass fraction N_0, where N is the mass fraction of the heavier species of the fluid mixture.

The upper free surface is assumed to be flat and subjected to a surface tension σ which varies linearly with temperature and mass concentration as:

$$\sigma(T', N) = \sigma_0\lfloor 1 - \gamma_T(T' - T'_0) - \gamma_N(N - N_0)\rfloor \quad (1)$$

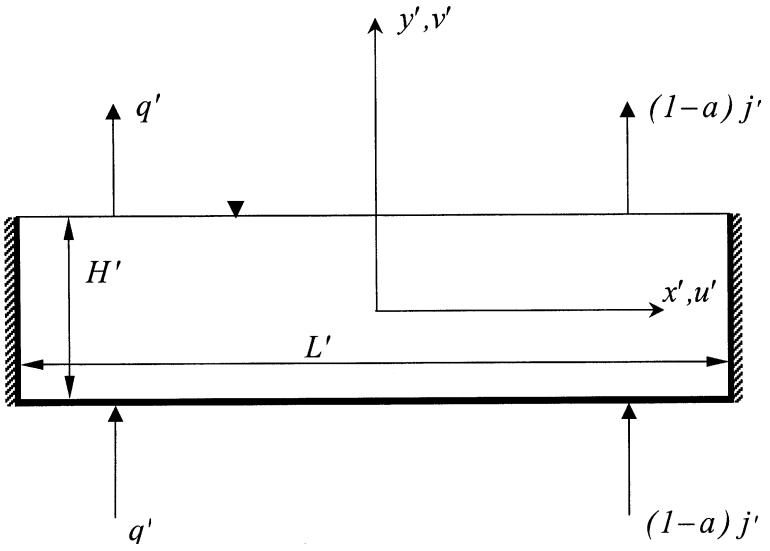

Fig. 1. Schematic diagram of the physical model and coordinate system.

where the subscript 0 refers to conditions at a reference state and γ_T and γ_N are the thermal and solutal expansion coefficients, respectively. For most fluids, γ_T is positive but γ_N may be positive or negative.

The phenomenological equations, relating the fluxes of heat $\vec{Q}'$ and matter $\vec{J}'$ to the thermal and solute gradients, present in a binary fluid mixture are given by (see for instance, De Groot and Mazur [19]):

$$\vec{Q}' = -k\nabla T', \quad \vec{J}' = -\rho D\nabla N - \rho D' N(1-N)\nabla T' \tag{2}$$

where ρ is the density of the mixture, k and D are the thermal conductivity and the isothermal diffusion coefficient. D' is the thermal diffusion coefficient. In the flux-gradient relation for heat the Dufour transport effect is not considered since it is negligible in liquids.

In the absence of gravity, the balanced equations for momentum, energy and mass fraction of the denser components are given below in terms of the vorticity ω', stream function Ψ' and velocity field $\vec{V}'$ as:

$$\frac{\partial \omega'}{\partial t'} + L(\Psi', \omega') = \nu\nabla^2\omega' \tag{3}$$

$$\frac{\partial T'}{\partial t'} + \vec{V}' \cdot \nabla T' = \alpha\nabla^2 T' \tag{4}$$

$$\frac{\partial N}{\partial t'} + \vec{V}' \cdot \nabla N = D\nabla^2 N + aD' N_0(1-N_0)\nabla^2 T' \tag{5}$$

where a is a real number, the significance of which will be discussed in the following text, $\omega' = -\nabla^2\Psi'$, $L(f,g) = f_y g_x - f_x g_y$. As usual, we have: $u' = \partial\Psi'/\partial y'$, $v' = -\partial\Psi'/\partial x'$ such that the mass conservation is satisfied.

In the above equations, ν is the kinematic viscosity of the mixture and α the thermal diffusivity coefficient. For reasonably dilute solutions, $N_0 \ll 1$ such that $(1-N_0) \approx 1$.

Hydrodynamic boundaries conditions include the no-slip requirement on the vertical walls and bottom of the cavity.

$$x' = \pm L'/2: \quad \Psi' = 0, \quad \frac{\partial\Psi'}{\partial x'} = 0 \tag{6a}$$

$$y' = -H'/2: \quad \Psi' = 0, \quad \frac{\partial\Psi'}{\partial y'} = 0 \tag{6b}$$

while the free upper surface hydrodynamic boundary conditions are:

$$y' = H'/2: \quad \Psi' = 0 \tag{6c}$$

$$\mu\frac{\partial u'}{\partial y'} = \frac{\partial\sigma}{\partial T'}\bigg|_N \frac{\partial T'}{\partial x'} + \frac{\partial\sigma}{\partial N}\bigg|_{T'} \frac{\partial N}{\partial x'} \tag{6d}$$

In the present investigation, it is assumed that the solutal forces prevailing in the binary mixture may be induced by two transport mechanisms. The first one is referred in literature as double diffusive convective problems. For this situation $a = 0$ and the species gradients are established by the imposition of given solutal boundary conditions (such as the constant mass fluxes j' considered here). The second one, for which $a = 1$, corresponds to the case where the concentration gradients, in a binary mixture initially homogeneous in composition, are due to the so-called thermal diffusion (or Soret) effects. The last term in the right hand side of Eq. (5) is a consequence of the Soret effect.

The boundary conditions applied on the horizontal boundaries of the system are uniform fluxes of heat and mass, per unit area, q' and $(1-a)j' = 0$ respectively.

The thermal boundary conditions considered here are:

$$x' = \pm L'/2: \quad \frac{\partial T'}{\partial x'} = 0 \tag{7a}$$

$$y' = \pm H'/2: \quad -k\frac{\partial T'}{\partial y'} = q' \tag{7b}$$

while those for the mass fraction are, for $a = 0$:

$$x' = \pm L'/2: \quad \frac{\partial N}{\partial x'} = 0 \tag{8a}$$

$$y' = \pm H'/2: \quad -\rho D\frac{\partial N}{\partial y'} = j' \tag{8b}$$

$$\text{and for } a = 1: \quad \left(\nabla N - \frac{D'}{D}N_0\nabla T'\right)\cdot\vec{n} = 0 \tag{9}$$

The above equation follows from Eq. (2b) and the fact that for Soret convection, it is assumed that all solid boundaries are impermeable ($\vec{J}'.\vec{n} = 0$). The unit vector $\vec{n}$ is perpendicular to a given boundary.

The following dimensionless variables (primed quantities are dimensional) are used:

$$\begin{aligned} &(x,y) = (x',y')/H', \quad u,v = (u',v')H'/\alpha, \\ &C = (N - N_0)/\Delta N \quad T = (T' - T_0)/\Delta T', \\ &\Delta T' = q'H'/k \quad t = t'\alpha/H'^2, \quad \Psi = \Psi'/\alpha \end{aligned} \tag{10}$$

where $\Delta N = j'H'/\rho D$ for double diffusion convection and $\Delta N = -N_0\Delta T'D'/D$ for Soret driven convection.

In terms of the above definitions, the dimensionless governing equations expressing conservation of momentum, energy and species reduce to the following equations:

$$\frac{\partial\omega}{\partial t} + L(\Psi,\omega) = Pr\nabla^2\omega \tag{11}$$

$$\frac{\partial T}{\partial t} + L(\Psi,T) = \nabla^2 T \tag{12}$$

$$\frac{\partial C}{\partial t} + L(\Psi,C) = \frac{1}{Le}(\nabla^2 C - a\nabla^2 T) \tag{13}$$

The dimensionless boundary conditions are given by:

$$x = \pm A/2: \quad \frac{\partial T}{\partial x} = \frac{\partial C}{\partial x} = 0, \quad \Psi = 0, \quad \frac{\partial\Psi}{\partial x} = 0 \tag{14a}$$

$$y = -1/2: \frac{\partial T}{\partial y} = \frac{\partial C}{\partial y} = -1, \quad \Psi = 0, \quad \frac{\partial\Psi}{\partial y} = 0 \tag{14b}$$

$$y = 1/2: \begin{cases} \dfrac{\partial T}{\partial y} = \dfrac{\partial C}{\partial y} = -1, \quad \Psi = 0 \\ \dfrac{\partial^2\Psi}{\partial y^2} = -\left(Ma_T\dfrac{\partial T}{\partial x} + \dfrac{Ma_S}{Le}\dfrac{\partial C}{\partial x}\right) \end{cases} \tag{14c}$$

The mass fraction boundary conditions are now observed to be independent of parameter a.

The above equations indicate that the present problem is governed by the following dimensionless parameters:

$$\begin{aligned} &Le = \frac{\alpha}{D}, \quad Pr = \frac{v}{\alpha}, \quad A = \frac{L'}{H'} \\ &Ma_T = -\left.\frac{\partial\sigma}{\partial T'}\right|_N \frac{\Delta T'H'}{\alpha\mu}, \quad Ma_S = -\left.\frac{\partial\sigma}{\partial N}\right|_{T'} \frac{\Delta NH'}{D\mu} \end{aligned} \tag{15}$$

It is noted from Eq. (14c) that the surface tension depends upon the thermal Marangoni number Ma_T and the solutal Marangoni number Ma_S.

The heat and mass transfer rates, defined in terms of the Nusselt and Sherwood numbers, are given by the following expressions:

$$Nu = \frac{1}{\Delta T}, \quad Sh = \frac{1}{\Delta C} \tag{16}$$

where $\Delta T = T(y = -1/2) - T(y = 1/2)$ and $\Delta C = C(y = -1/2) - C(y = 1/2)$ are the temperature and concentration differences, evaluated between the horizontal boundaries. All the numerical values for Nu and S, reported in this study, are evaluated at the position x for which the stream functions is the maximum.

3. Numerical solution

The solution of the governing equations and boundary conditions, Eqs. (11)–(14) is obtained using a control volume approach and the SIMPLER algorithm (Patankar [20]). A finite difference procedure with variable grid size is used for better consideration of boundary conditions especially near the surface tension. The power-law scheme is used to evaluate the flow, heat and mass fluxes across each of the control volume boundaries. A second order backwards finite difference scheme is employed to discretize the temporal terms appearing in the governing equations. The discretized momentum, energy and concentration equations are underrelaxed to accelerate the convergence. The relaxation parameter was chosen equal to 0.5. A Thomas iterative procedure is employed to solve the resulting discretized equations. At each new time step, the updating of the physical new variables is done until the convergence criterion $\sum_{i=1}^{m}(b_i^k - b_i^{k-1})/\sum_{i=1}^{m} b_i^k \leqslant 10^{-9}$ is satisfied, where b stands for Ψ, T and C.

Numerical tests have been performed to determine the minimum aspect ratio above which the flow can be assumed to be parallel. In the range of the parameters considered in this investigation it was found that the numerical results can be considered independent of the aspect ratio when $A \geqslant 6$. For this reason most of the numerical results reported here were obtained for $A = 8$ with typically 60×180 mesh points.

The numerical results presented in this study are limited to water-based solutions, i.e. $Pr = 7$. However, it is well known that the solution is rather insensible to the

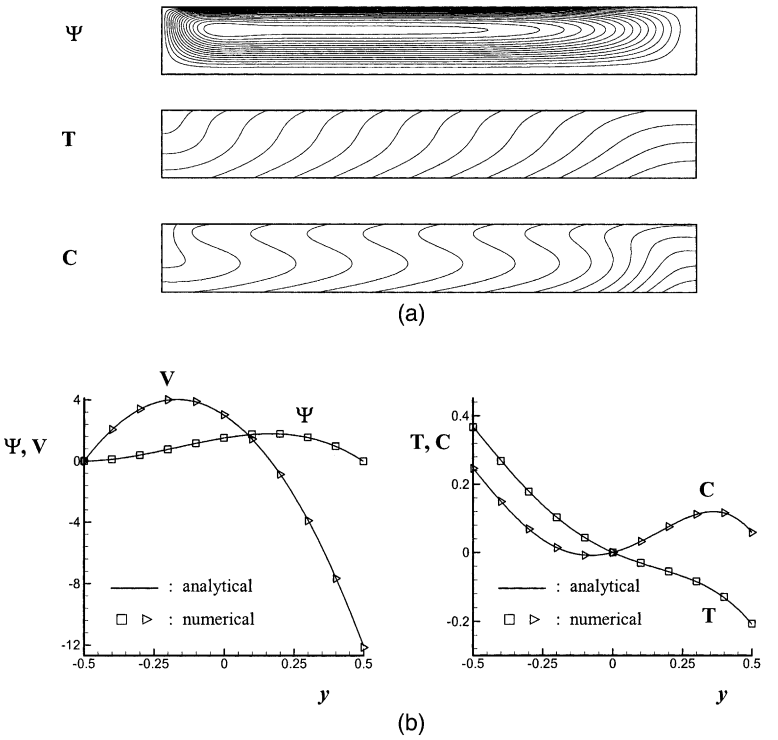

Fig. 2. (a) Streamlines, isotherms and isoconcentrates. (b) Streamfunction, velocity, temperature and concentration for $A = 8$, $\overline{M}a_T = 2.5$, $\overline{M}a_S = -0.5$, $Le = 2$ and $a = 1$; $\Psi_{Max} = 1.79$, $Nu = 1.73$, $Sh = 5.32$.

Prandtl number provided that this latter is of order one or greater. This finding is also confirmed by the present analytical solution which, in its range of validity, is independent of Pr.

Typical numerical results are presented in Fig. 2 for $A = 8$, $\overline{M}a_T = 2.5$, $\overline{M}a_S = -0.5$, $Le = 2$ and $a = 1$ (Soret driven convection). In Fig. 2a, streamlines, isotherms and isoconcentrates are presented from top to bottom. The results clearly illustrate the fact that for a shallow cavity ($A \gg 1$) the flow in the core region of the enclosure is essentially unicellular and parallel because of the Neumann boundary conditions considered here, while the temperature and concentration in the core are linearly stratified in the horizontal directions. The analytical solution, developed in the following section, will rely on these observations. The numerically determined profiles of streamfunction, velocity, temperature and concentration at the center of the convective cell are compared in Fig. 2b with their analytical counterparts derived below. The agreement between the two solutions is seen to be excellent.

4. Analytical solution

In this section, an analytical solution is developed for steady-state flows using the parallel flow approximation, which leads to the following simplifications:

$$\Psi(x,y) = \Psi(y), \quad T(x,y) = C_T x + \theta(y),$$
$$C(x,y) = C_S x + Z(y) \tag{17}$$

where C_T and C_S are unknown constant gradients respectively in x direction.

Using these approximations together with boundary conditions (14b) and (14c), Eqs. (11)–(13) are reduced to a set of ordinary differential equations which can be solved to yield a closed form analytical solution. It is found that:

$$\Psi(y) = -\Psi_0(8y^3 + 4y^2 - 2y - 1) \tag{18}$$

$$\theta(y) = -C_T \Psi_0 y f(y) - y \tag{19}$$

$$Z(y) = -(LeC_S + aC_T)\Psi_0 y f(y) - y \tag{20}$$

where $f(y) = 2y^3 + 4y^2/3 - y - 1$, $\Psi_0 = 3(\overline{M}a_T C_T + \overline{M}a_S C_S/Le)/2$ and $\overline{M}a_i = Ma_i/Ma^{sup}$ with $Ma^{sup} = 48$.

The values of C_T and C_S are obtained using the fact that the heat and solute transports across a vertical section at any x should be zero, yielding:

$$C_T = \frac{4}{3}\frac{b^2\Psi_0}{2b^2 + \Psi_0^2},$$
$$C_S = \frac{4}{3}b^2\Psi_0\frac{(2b^2 + \Psi_0^2)Le + a(2b^2 - Le\Psi_0^2)}{(2b^2 + \Psi_0^2)(2b^2 + Le^2\Psi_0^2)} \tag{21}$$

where $b^2 = 105/128$. It is noted that the values of C_T and C_S can be obtained explecitely only for the thermal and solutal boundary conditions considered here.

Substituting these results into Eq. (16), we can deduce the expressions for Nusselt, Nu, and Sherwood, Sh, numbers as follows:

$$Nu = -\frac{9\left(2b^2 + \Psi_0^2\right)}{\Psi_0^2(8b^2 - 9) - 18b^2} \tag{22}$$

$$Sh = -\frac{9\left(2b^2 + Le^2\Psi_0^2\right)}{Le^2\Psi_0^2(8b^2 - 9) - 18b^2 + a\frac{16b^4\Psi_0^2(1+Le)}{2b^2+\Psi_0^2}} \tag{23}$$

Substituting C_T and C_S into Ψ_0 it is found that:

$$\Psi_0[Le^4\Psi_0^4 - 2b^2 d_1 Le^2\Psi_0^2 - b^4 d_2] = 0 \tag{24}$$

where

$$d_1 = Le^2(\overline{M}a_T - 1) + \overline{M}a_S(1 - a) - 1,$$
$$d_2 = 4Le^2[\overline{M}a_S(1 + a/Le) + \overline{M}a_T - 1] \tag{25}$$

The solution for Eq. (24) is expressed as follows:

$$\Psi_0 = \pm\frac{b}{Le}\sqrt{d_1 \pm \sqrt{d_1^2 + d_2}} \tag{26}$$

The supercritical Marangoni number $(\overline{M}a_T)_c^{sup}$, for the onset of motion from the rest state, is obtained, when the conditions $d_1 < 0$ and $d_2 = 0$ are satisfied, as:

$$(\overline{M}a_T)_c^{sup} = 1 - \overline{M}a_S(1 + a/Le) \tag{27}$$

In the present analysis, it can be demonstrated that subcritical flows occur when $d_1 > 0$ and $d_2 < 0$ and more precisely when:

$$\overline{M}a_S < \frac{1 - \overline{M}a_T}{1 + a/Le} \quad \text{and} \quad Le > \sqrt{\frac{\overline{M}a_S(1 - a) - 1}{1 - \overline{M}a_T}} \tag{28}$$

We can deduce, from the above expressions, the following specific conditions for the existence of the subcritical flows.

$$\overline{M}a_S < 0 \quad \text{and} \quad Le > \sqrt{\frac{(1 - a)\overline{M}a_S - 1}{(1 + a/Le)\overline{M}a_S}} \tag{29}$$

The subcritical Marangoni number $(\overline{M}a_T)_c^{sub}$, for the onset of motion at finite amplitude convection is obtained from the conditions $d_1 > 0$ and $d_1^2 + d_2 = 0$ as:

$$(\overline{M}a_T)_c^{sub} = 1 + \frac{\overline{M}a_S(a - 1) - 1 + 2\sqrt{\overline{M}a_S[-Le(Le + a) + 1 - a]}}{Le^2} \tag{30}$$

where

$$\overline{M}a_S < 0 \quad \text{and} \quad \overline{M}a_S[-Le(Le + a) + 1 - a] > 0 \tag{31}$$

From the present solution, which is valid asymptotically for both $A \gg 1$ and $Pr \gg 1$, it is clear that the present problem is now governed only by three parameters, namely the thermal Marangoni number Ma_T, the solutal Marangoni number Ma_S and the Lewis number Le. For positive values of Ma_T and Ma_S, both the temperature and concentration effects are destabilizing. Naturally, in general, the Marangoni numbers can have opposite signs.

Typical bifurcation diagrams for the steady-state solution are presented in Figs. 3 and 4 for various values of the solutal Marangoni numbers ($Ma_S = -200$, 0 and 200; i.e. $\overline{M}a_S = -4.17$, 0 and 4.17), for $Le = 2$ and $a = 0$ (double diffusion) and $a = 1$ (Soret effect), respectively. The thermal and solutal Marangoni numbers are normalized with respect to the critical parameter $Ma^{sup} = 48$. The curves depicted in those graphs are the result of the present theory, the solid lines corresponding to stable branches and the dotted ones to unstable branches. The numerical solution of the full governing equations, obtained for $A = 8$, depicted by dots, are seen to be in good agreement with the analytical solution.

Pure thermal Marangoni convection in a horizontally infinite layer of a fluid can be deduced from the present analysis. Thus, substituting $\overline{M}a_S = 0$ in Eqs. (18)–(27), leads to the fundamental equations ruling this case. For this situation, it is found that convection is possible only for $\overline{M}a_T \geqslant 1$. This result is in agreement with the linear stability analysis of Nield [4] from which it was demonstrated that, for the thermal and solutal boundary conditions considered here, the onset of convection occurs at zero wave number. Thus, it is not surprising that the present parallel flow approximation is capable to predict the onset of motion.

The results obtained for double diffusive convection, Fig. 3, and Soret induced convection, Fig. 4, will be discussed simultaneously since they are qualitatively similar. Figs. 3a and 4a illustrate the effect of $\overline{M}a_T$ on Ψ_{Max} for typical values of $\overline{M}a_S$. For $\overline{M}a_S = 0$, as discussed above, the onset of convection occurs at $(\overline{M}a_T)_c^{sup} = 1$, through a pitchfork bifurcation. The curves corresponding to $\overline{M}a_S = 4.17$ ($\overline{M}a_S = 200$) illustrate the situation where both thermal and solutal contributions are destabilizing ($Ma_T > 0$ and $Ma_S > 0$). The results indicate that the onset of convection occurs at a $(\overline{M}a_T)_c^{sup}$ lower than that for the pure thermal one ($(\overline{M}a_T)_c^{sup} = 1$). Two distinct convective regimes are noticed. The first one, corresponding to relatively weak flows, occurs for $\overline{M}a_T$ between the thermal-solutal and the thermal thresholds. The second one, observed for $\overline{M}a_T$ higher than the thermal threshold, is relatively stronger and similar to the one observed for pure thermal situation. On the other hand the curves corresponding to $\overline{M}a_S = -4.17$ illustrate the situation where thermal contributions are destabilizing while the solutal ones are stabilizing. For this situation, the onset of

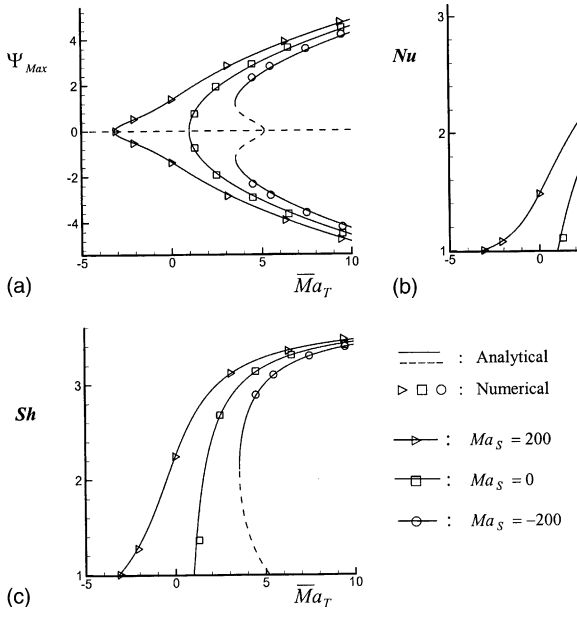

Fig. 3. Bifurcation diagrams for $Le = 2$, $a = 0$, for $\overline{M}a_S = 4.17$, 0 and −4.17 for (a) Ψ_{Max} versus $\overline{M}a_T$; (b) *Nu* versus $\overline{M}a_T$; (c) *Sh* versus $\overline{M}a_T$.

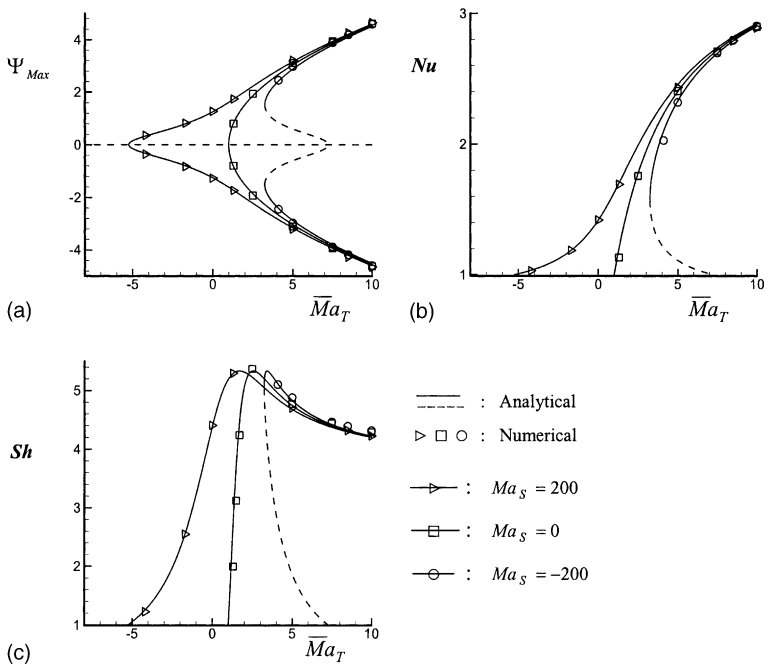

Fig. 4. Bifurcation diagrams for $Le = 2$, $a = 1$, for $\overline{M}a_S = 4.17$, 0 and −4.17 for (a) Ψ_{Max} versus $\overline{M}a_T$; (b) *Nu* versus $\overline{M}a_T$; (c) *Sh* versus $\overline{M}a_T$.

convection occurs with a finite amplitude convection at a subcritical thermal Marangoni number predicted by Eq. (30). Thus, for the parameters considered here, $(\overline{M}a_T)_c^{sup} = 3.56$ when $a = 0$ and $(\overline{M}a_T)_c^{sup} = 3.25$ when $a = 1$. These points correspond to saddle-node bifurcations, where two branches emerge. An unstable branch, represented by a dashed line, connects the subcritical Marangoni number to the supercritical Marangoni

number predicted by Eq. (27). The other branch, represented by a solid line, is stable. Similar results have been reported by Bergeron et al. [16].

Figs. 3 and 4 also exemplify the effects of $\overline{M}a_T$ and $\overline{M}a_S$ on the heat and mass transfer. Thus, it is observed from Fig. 4b and c that, when compared with the pure thermal situation ($\overline{M}a_S = 0$), the Nusselt number Nu is higher when the solutal and thermal influences are both destabilizing than when a stabilizing solutal Marangoni, competing with a destabilizing thermal Marangoni, is considered. It is noticed that, for very large values of $\overline{M}a_T$, all the curves tend asymptotically towards a constant value given by:

$$Nu = Sh = \frac{1}{1 - 8b^2/9} \approx 3.69 \tag{32}$$

as it can be deduced from Eqs. (22) and (23). This behavior is a consequence of the particular boundary conditions considered here (Neumann conditions).

Results obtained for the mass transfer are depicted in Figs. 3c and 4c. The Sherwood number in the case of Soret induced convection ($a = 1$) is observed to be quite different from that obtained in the case of double diffusive convection ($a = 0$). Thus, it is seen from Fig. 4c that Sh first passes through a maximum value before decreasing asymptotically toward the constant value 3.69 when $\overline{M}a_S$ is made sufficient large. This is not the case when $a = 0$ for which Fig. 3c indicates that Sh increases monotonously towards the constant value 3.69. It is noted that the significance of Sh in both cases is different. The Sherwood number, for double diffusive convection, represents the mass transfer across the horizontal boundaries of the layer resulting from the combined action of convection and conduction. On the other hand, the Sherwood number, for Soret induced convection, has not the same interpretation. Since the boundaries of the layer are impermeable, Sh is rather related to the concentration distribution induced by the Soret effect and by convection.

Another view of the effects of opposing and aiding thermal and solutal Marangoni numbers is presented in Fig. 5 for $Le = 2$. Here again, the results obtained for the case $a = 0$ (Fig. 5a) and $a = 1$ (Fig. 5b) are qualitatively similar and will be discussed simultaneously. When $\overline{M}a_T = 0$ (pure solutal situation), convection occurs at $\overline{M}a_S = 1/(1 + a/Le)$, as predicted by Eq. (27), and convection is possible only for $\overline{M}a_S > 0$, i.e. when the solutal influence is destabilizing. For $\overline{M}a_T = -4.17$ ($Ma_T = -200$), i.e. when the thermal influence is stabilizing, here again convection is possible only when $\overline{M}a_S > 0$, i.e. when the solutal influence is destabilizing. For this situation, the onset of convection also occurs through a pitchfork bifurcation. On the other hand, when $\overline{M}a_T = -4.17$ ($Ma_T = -200$), i.e. when the thermal influence is destabilizing, convection is possible only for

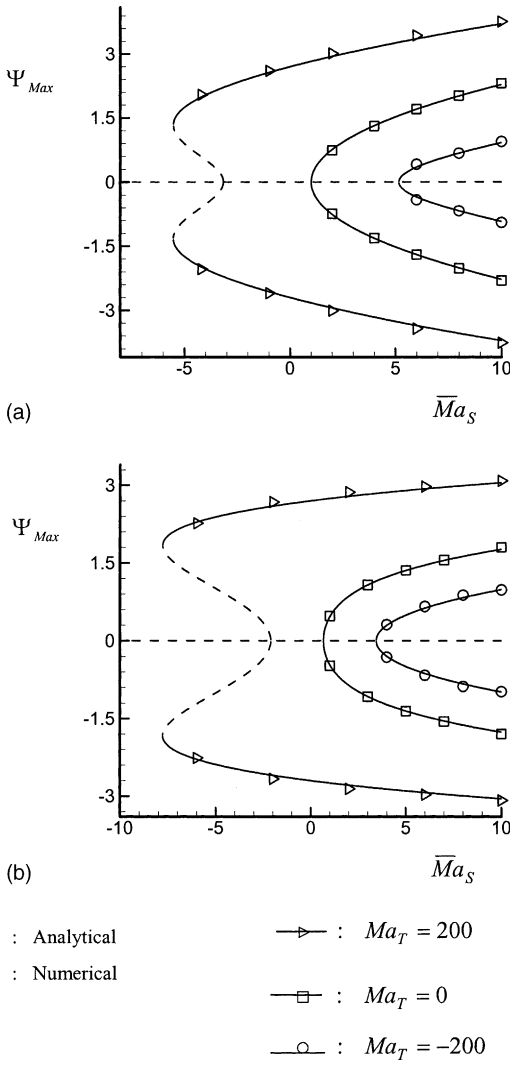

Fig. 5. Bifurcation diagrams in terms of Ψ_{Max} versus $\overline{M}a_S$ for $Le = 2$ and for (a) double diffusive convection and (b) Soret induced convection.

$\overline{M}a_S = -5.52$ ($a = 0$) and $\overline{M}a_S = -7.78$ ($a = 1$). At this point, where the solutal influence is stabilizing ($\overline{M}a_S < 0$), convection occurs with a finite amplitude convection at a subcritical Marangoni number predicted by Eq. (30).

The effect of the Lewis number on the present problem is illustrated in Fig. 6 for $\overline{M}a_S = -2.08$, i.e. when the solutal influence is stabilizing. Fig. 6a shows the bifurcation curves, obtained for double diffusive convection ($a = 0$), in terms of the flow intensity Ψ_{Max} as a function of $\overline{M}a_T$ ($\overline{M}a_T > 0$, i.e. for a destabilizing thermal influence). For these conditions, according to Eq. (29), the Lewis number expressing the transition from a supercritical to a subcritical bifurcation is

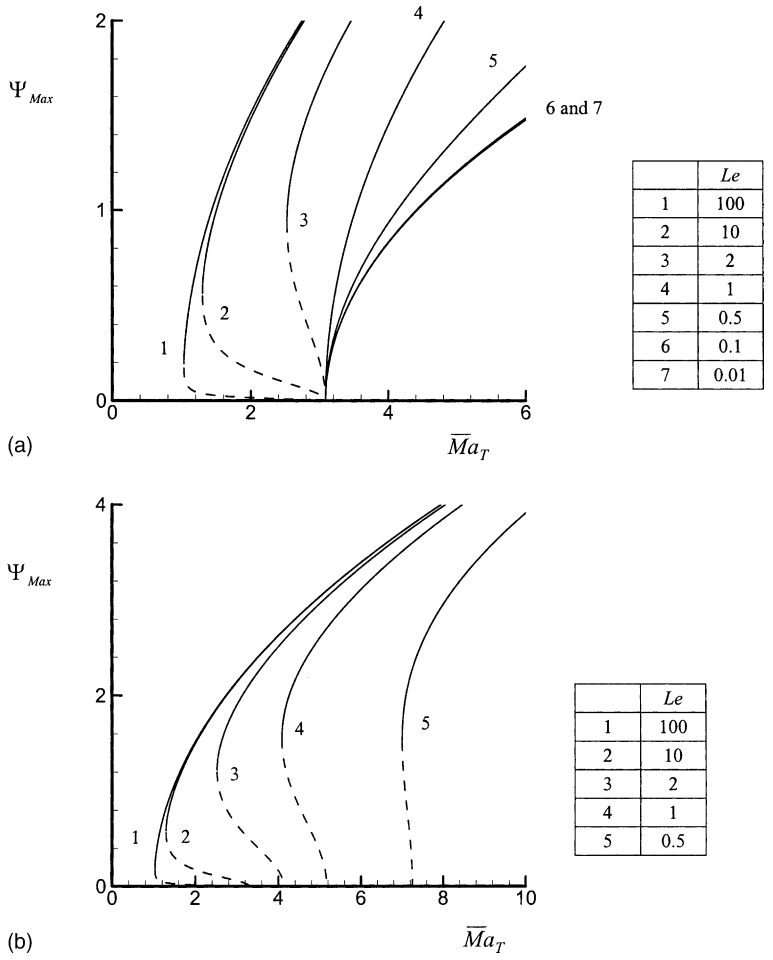

	Le
1	100
2	10
3	2
4	1
5	0.5
6	0.1
7	0.01

	Le
1	100
2	10
3	2
4	1
5	0.5

Fig. 6. Bifurcation diagrams in terms of Ψ_{Max} versus $\overline{Ma}_{\mathrm{T}}$ for $\overline{Ma}_{\mathrm{S}} = -2.08$ and different Lewis numbers for (a) double diffusive convection and (b) Soret induced convection.

$Le = 1.22$. As it can be observed from the graphs, the bifurcation is supercritical when $Le < 1.22$ (i.e. $Le = 1$) and subcritical when $Le < 1.22$ ($Le = 2$, 10 and 100). The limiting curve corresponding to $Le \to \infty$ ($Le = 100$) is also presented on the graph for comparison. For this situation, the solute concentration is almost uniform on the whole of the layer, except in very thin layers near the horizontal boundaries. For this limit, it is observed that the critical Marangoni number for the onset of convection approaches that corresponding to a pure thermal situation, i.e. $(\overline{Ma}_{\mathrm{T}})_c^{\mathrm{sub}} \to 1$ and $\Psi_{\mathrm{Max}} \to 0$ as $Le \to \infty$. In this case of high value of the Lewis number, we can deduce from Eq. (26) the following simplification for Ψ_0:

$$\Psi_0 = \pm b\sqrt{2(\overline{Ma}_{\mathrm{T}} - 1)} \tag{33}$$

Fig. 6b shows the corresponding curves obtained for $a = 1$, i.e. for Soret induced convection. The results are observed to be quite different. Thus, according to Eq. (29), it is predicted that the Lewis number expressing the transition from supercritical to subcritical bifurcation is $Le = 0.35$, such that all the curves presented in the graph indicate the occurrence of subcritical convection. Also, it is noticed that the onset of supercritical convection is now function of the Lewis number, as predicted by Eq. (27). Here again, the limiting case $Le \to \infty$ corresponds to the pure fluid situation.

Fig. 7 presents a bifurcation diagram in terms of Ψ_{Max} versus Le for $\overline{Ma}_{\mathrm{T}} = 4.17$ and $\overline{Ma}_{\mathrm{S}} = -2.08$. In the case of double diffusive convection, it is observed that convection is possible for any value of the Lewis number since, with the parameters considered here, Eq. (29) is satisfied independently of the value of Le. However, for Soret induced convection, the onset of supercritical convection occurs at $Le = 1.92$. Furthermore, according to Eq. (29), the Lewis number for the onset of subcritical convection is $Le = 0.35$. As a result, Soret induced convection, for the parameters considered here,

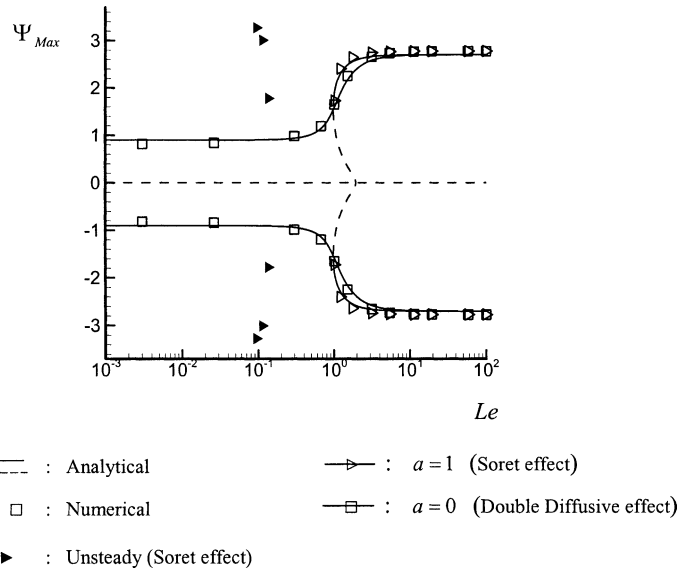

Fig. 7. Bifurcation diagrams in terms of Ψ_{Max} versus Le for $\overline{Ma}_{\mathrm{T}} = 4.17$ and $\overline{Ma}_{\mathrm{S}} = -2.08$ for double diffusive convection and Soret induced convection.

is possible only for $Le \geqslant 0.35$. For very large values of Le, it is noted that, in agreement with the results given by Eq. (29), the solution becomes independent of the parameter a, i.e. of the mechanism responsible for the establishment of the density gradients. Thus, in both cases, $\Psi_{\mathrm{Max}} \to 2.70$. Also, it is observed that for $Le \to 0$, $\Psi_{\mathrm{Max}} \to 0.90$.

5. Linear stability analysis

In this section, the stability of the convective flows, predicted by parallel flow approximations, is investigated using the linear stability analysis. At the very beginning of instability of the basic flow state, the global flow can be assumed to be a superposition of the basic flow and of an infinitesimal perturbation that can be developed into normal modes as follows:

$$\begin{aligned}\widetilde{\Psi}(t,x,y) &= \widetilde{\Psi}(y)\mathrm{e}^{pt+k(x\cos\phi+z\sin\phi)}\\ \tilde{\theta}_{\mathrm{T}}(t,x,y) &= \tilde{\theta}_{\mathrm{T}}(y)\mathrm{e}^{pt+k(x\cos\phi+z\sin\phi)}\\ \tilde{\theta}_{\mathrm{S}}(t,x,y) &= \tilde{\theta}_{\mathrm{S}}(y)\mathrm{e}^{pt+k(x\cos\phi+z\sin\phi)}\end{aligned} \tag{34}$$

where $p = (\sigma + \mathrm{i}\omega)$ and σ, and ω are respectively the perturbation temporal growth rate and frequency. The wave number k is real since the system is supposed to be infinite in the horizontal direction and the perturbations are bounded. The parameter ϕ is the direction of propagation of the traveling waves. Inserting these perturbation fields into the flow fields described by Eqs. (11)–(13) and linearizing about the basic flow state yields the following set of equations:

$$Pr(D^2-k^2)^2\widetilde{\Psi} - \mathrm{i}k\psi'(y)(D^2-k^2)\widetilde{\Psi} + \mathrm{i}k\psi'''(y)\widetilde{\Psi} = p(D^2-k^2)\widetilde{\Psi} \tag{35}$$

$$(D^2-k^2)\tilde{\theta}_{\mathrm{T}} - \mathrm{i}k\psi'(y)\tilde{\theta}_{\mathrm{T}} - C_{\mathrm{T}}D\widetilde{\Psi} + \mathrm{i}k\theta'(y)\widetilde{\Psi} = p\tilde{\theta}_{\mathrm{T}} \tag{36}$$

$$\frac{1}{Le}(D^2-k^2)(\tilde{\theta}_{\mathrm{S}} - a\tilde{\theta}_{\mathrm{T}}) - \mathrm{i}k\psi'(y)\tilde{\theta}_{\mathrm{S}} - C_{\mathrm{S}}D\widetilde{\Psi} + \mathrm{i}kZ'(y)\widetilde{\Psi} = p\tilde{\theta}_{\mathrm{S}} \tag{37}$$

The corresponding boundary conditions are:

$$y = -1/2: \quad \frac{\mathrm{d}\tilde{\theta}_{\mathrm{T}}}{\mathrm{d}y} = \frac{\mathrm{d}\tilde{\theta}_{\mathrm{S}}}{\mathrm{d}y} = 0, \quad \widetilde{\Psi} = 0, \quad \frac{\mathrm{d}\widetilde{\Psi}}{\mathrm{d}y} = 0 \tag{38a}$$

$$y = 1/2: \begin{cases} \dfrac{\mathrm{d}\tilde{\theta}_{\mathrm{T}}}{\mathrm{d}y} = \dfrac{\mathrm{d}\tilde{\theta}_{\mathrm{S}}}{\mathrm{d}y} = 0, \quad \widetilde{\Psi} = 0 \\ \dfrac{\mathrm{d}^2\widetilde{\Psi}}{\mathrm{d}y^2} = -ik\left(Ma_{\mathrm{T}}\tilde{\theta}_{\mathrm{T}} + \dfrac{Ma_{\mathrm{S}}}{Le}\tilde{\theta}_{\mathrm{S}}\right) \end{cases} \tag{38b}$$

where $D = \mathrm{d}/\mathrm{d}y$ and $\psi'(y)$, $\psi'''(y)$, $\theta'(y)$, $Z'(y)$ are derivatives of stream function, temperature and concentration of the basic flow.

As the system of Eqs. (35)–(37) contains the basic flow velocity $u(y) = \Psi'(y)$, we may expect the occurrence of hydrodynamic modes due to destabilization of the velocity profile. For the two-dimensional parallel flow $u(y)$ considered here, the minimum critical unstable Ma_{T}

number occurs for a two-dimensional disturbance propagating along the same direction ($\phi = 0$) (Squire's theorem [21]).

The perturbed state Eqs. (35)–(37) together with the homogeneous boundary conditions (38) may be written in a compact matrix form:

$$L(k)\vec{Y} = pM(k)\vec{Y} \tag{39}$$

where $\vec{Y} = [\tilde{\Psi}(y), \tilde{\theta}_T(y), \tilde{\theta}_S(y)]$ is a three-component vector of the perturbation (stream function, temperature and concentration); $L(k)$ and $M(k)$ are two linear differential operators that depend on the control parameters of the problem.

The system of Eq. (39) is solved numerically using a finite difference scheme. The system is discretized in the domain between $y = -1/2$ and $1/2$, and written in the form $L_{ij}(k)\vec{Y}_j = pM_{ij}(k)\vec{Y}_j$. Using a standard subroutine for the eigenvalue problem such as EIGENC of IMSL, the eigenvalues are determined as a function of the control parameters, Ma_T, Ma_S, Le, a, and the wave number k. For given values of Ma_T, Ma_S, Le and a, the value of Ma_T is evaluated for which the fastest growth rate (maximal value of σ) cancels. This gives a functional $Ma_T = Ma_T(k, \varpi)$. The minimum in the marginal stability curve $Ma_T(k)$ determines the critical state parameters (k, ϖ, Ma_{TC}). The critical parameter value is seen to converge well for a discritization number $N > 60$.

Fig. 8 illustrates typical results concerning the stability of the parallel flow approximation as predicted by the present numerical procedure. Results are presented, for $Le = 2$ and 10, in terms of the thermal Marangoni number versus the solutal Marangoni number for both the cases $a = 0$ and $a = 1$. The onsets of convection from the rest state, are also indicated in the graphs for completeness. Fig. 8a shows that, in the case of double diffusive convection, the influence of the Lewis number on the occurrence of Hopf's bifurcations, depends strongly upon the value of $\overline{Ma}_S$. Thus, for $\overline{Ma}_S > 0$, the parallel flow becomes unstable earlier as the value of the Lewis number is made smaller. The reverse effect is observed for $\overline{Ma}_S < 0$. In the case of Soret induced convection it is noticed that the effect of Le is considerable. Thus, for $Le = 2$, Fig. 8b indicates that, according to the linear stability theory, the parallel flow solution is almost unconditionally stable, excepted in a thin region in the vicinity of $\overline{Ma}_S \geqslant 0$. However it is noted that this region is extended to negative values of $\overline{Ma}_S$ ($\overline{Ma}_S \approx -3.87$) and large positive values of $\overline{Ma}_S$ as the value of the Lewis number is increased to $Le = 10$.

The effects of the Lewis number on the critical thermal Marangoni numbers for Hopf bifurcations are illustrated in Fig. 9 for both $a = 0$ and $a = 1$. Fig. 9a shows the results obtained for $\overline{Ma}_S = 2.08$. As discussed

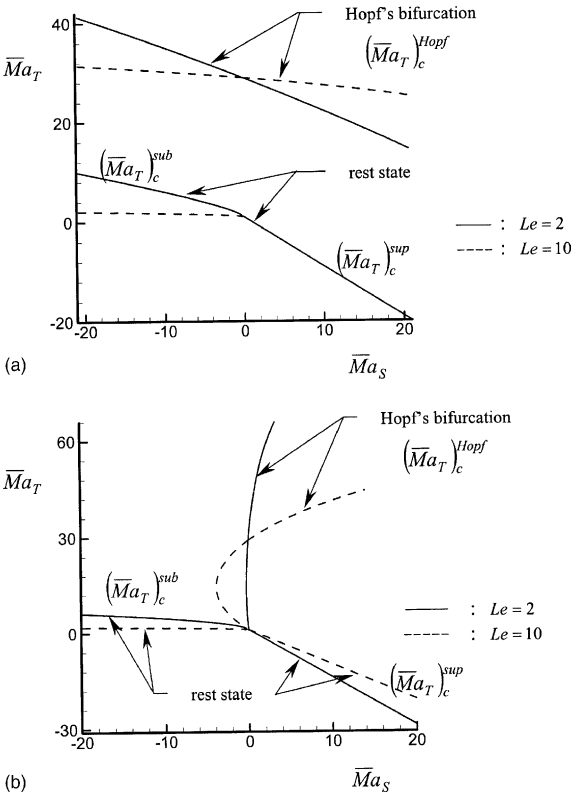

Fig. 8. Bifurcation diagram in terms of $\overline{Ma}_T$ versus $\overline{Ma}_S$ for (a) double diffusive convection and (b) Soret induced convection.

earlier, for $\overline{Ma}_S > 0$, the onset of convection from the rest state occurs through a supercritical Marangoni number, Eq. (27). For double diffusive convection, $(\overline{Ma}_T)_c^{sup} = -1.08$ independently of the Lewis number while for Soret induced convection, it is seen that $(\overline{Ma}_T)_c^{sup}$ depends strongly upon Le. The effect of Le on $(\overline{Ma}_T)_c^{Hopf}$ is also observed to be important. According to the linear stability analysis, the parallel flow is, for the value of $\overline{Ma}_S$ considered here, unconditionally stable for $Le \leqslant 0.15$ for $a = 0$. For $a = 1$, the results indicate that the critical Marangoni number for Hopf bifurcation increases considerably as the value of Le is decreased. On the other hand, for $Le \geqslant 40$, it is observed that the results become independent of a. Fig. 9b displays the results obtained for $\overline{Ma}_S < 0$ for which the onset of convection from the rest state occurs for relatively low Lewis numbers, through a supercritical Marangoni number. Also included in the graphs the overstable Marangoni number $(\overline{Ma}_T)_c^{over}$ obtained by considering the linear stability of the rest state with present numerical procedure (the details are not discussed here). As the value of Le is increased, the onset of motion is characterized by a subcritical Marangoni number. The range of Lewis numbers for which these two types of convection

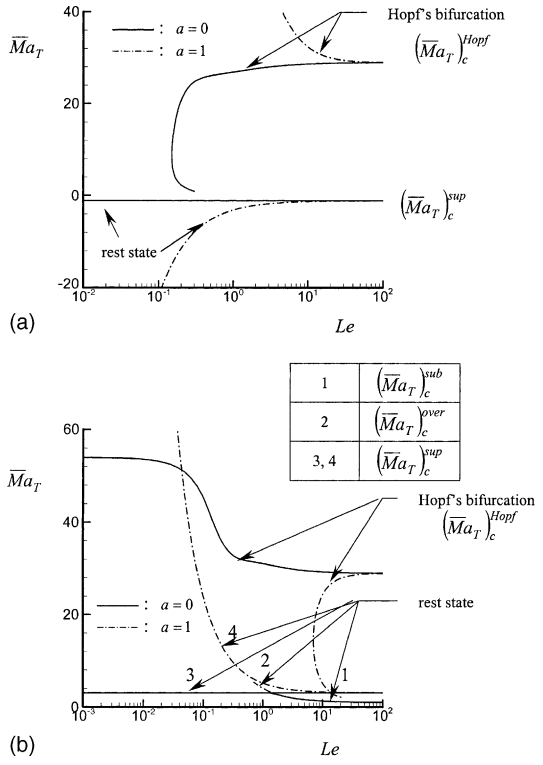

Fig. 9. Bifurcation diagram in terms of $\overline{M}a_T$ versus Le, for (a) $\overline{M}a_S = 2.08$ and (b) $\overline{M}a_S = -2.08$.

are observed depends considerably of the value of a. The numerically determined critical Marangoni numbers for Hopf bifurcations indicate that for $a = 0$, a value of $(\overline{M}a_T)_c^{Hopf}$ always exists, independently of the value of Le. However, for $a = 1$, the existance $(\overline{M}a_T)_c^{Hopf}$ is possible only for $Le > 7.01$. Here again, for $Le \to \infty$, the results are independent of the value of Le.

6. Conclusion

Marangoni convection in a horizontal layer of a binary fluid has been investigated for both double diffusive and Soret induced convection. The partial differential equations governing the problem are solved using a control volume approach. An analytical solution is obtained assuming that the flow field in the core of the cavity is parallel to the horizontal boundaries. The main conclusions of the present analysis are as follows:

1. The onsets of supercritical and subcritical convection have been determined analytically in terms of the governing parameters of the problem. Domains of existence of the different regimes were found to depend on the thermal and solutal Marangoni numbers and on the Lewis number.
2. The parallel flow approximation was found to be in good agreement with the numerical results, independently of the strength of the convective motion, in the range of the parameters considered in this study.
3. Far from criticality, a stability analysis of the parallel flow solution has been carried out and the thresholds for Hopf bifurcations obtained numerically.

References

[1] S. Ostrach, Fluid mechanics in crystal growth—the 1982 Freeman scholar lecture, J. Fluids. Eng. 105 (1983) 5–20.
[2] S. Ostrach, Low-gravity fluid flows, Ann. Rev. Fluid Mech. 14 (1982) 313–345.
[3] J.R.E. Pearson, On convective cells induced by surface tension, J. Fluid Mech. 4 (1958) 489–500.
[4] D.A. Nield, Surface tension and buoyancy effect in cellular convection, J. Fluid. Mech. 19 (1964) 341–354.
[5] S.H. Davis, G.M. Homsy, Energy stability theory for free-surface problem: buoyancy-thermocapillary layers, J. Fluid Mech. 53 (1972) 305–327.
[6] L.E. Scriven, C.S. Sternling, On cellular convection driven by surface-tension gradients: effects of mean surface tension and surface viscosity, J. Fluid Mech. 19 (1964) 321–340.
[7] M. Takashima, Surface tension driven instability in a horizontal liquid layer with a deformable free surface. I. Stationary convection, J. Phys. Soc. Jpn. 50 (1981) 2745–2750.
[8] P.C. Dauby, G. Lebon, Bénard–Marangoni instability in rigid rectangular containers, J. Fluid Mech. 329 (1996) 25–64.
[9] A. Bergeon, D. Henry, E. Knobloch, Three-dimensional Marangoni–Bénard flows in square and nearly square containers, J. Phys. Fluids, A 13 (2001) 92–98.
[10] H. Tomita, K. Abe, Numerical simulation of pattern formation in the Bénard–Marangoni convection, Phys. Fluids 12 (2000) 1389–1400.
[11] C.L.M. Mc Taggart, Convection driven concentration and temperature-dependent surface tension, J. Fluid Mech. 134 (1983) 301–310.
[12] K.L. Ho, H.S. Chang, On nonlinear doubly-diffusive Marnagoni instability, AIChE J. 34 (1988) 705–722.
[13] C.F. Chen, T.S. Su, Effect of surface tension on the onset of convection in a doubly-diffusive layer, Phys. Fluids A 4 (11) (1992) 2360–2366.
[14] S.W. Joo, Marangoni instabilities in liquid mixtures with Soret effects, J. Fluid Mech. 293 (1995) 127–145.
[15] A. Bergeron, D. Henry, H. Benhadid, Marangoni–Bénard instability in microgravity with Soret effect, Int. J. Heat Mass Transfer 37 (11) (1994) 1545–1562.
[16] A. Bergeron, D. Henry, H. Benhadid, L.S. Tuckerman, Marangoni convection in binary mixtures with Soret effect, J. Fluid Mech. 375 (1998) 143–177.

[17] T.C. Jue, Numerical analysis of thermosolutal Marangoni and natural convection flows, Num. Heat Transfer 34 (1998) 652–663.
[18] K. Arafune, A. Hirata, Interaction solutal and thermal Marangoni convection in a rectangular open boat, Num. Heat Transfer 34 (1998) 421–429.
[19] S.R. De Groot, P. Mazur, Non equilibrium thermodynamics, North Holland, 1969.
[20] S.V. Patankar, Numerical Heat Transfer and Fluid Flow, Hemisphere Publishing Co, 1980.
[21] P.G. Drazin, W.H. Reid, Hydrodynamic Stability, Cambridge University Press, 1991.